Biosensors and Bioelectronics 180 (2021) 113116

Contents lists available at ScienceDirect

Biosensors and Bioelectronics

journal homepage: http://www.elsevier.com/locate/bios

Gold nanostructured laser-scribed graphene: A new electrochemical biosensing platform for potential point-of-care testing of disease biomarkers

Sakandar Rauf [1], Abdellatif Ait Lahcen [1], Abdulrahman Aljedaibi, Tutku Beduk, José Ilton de Oliveira Filho, Khaled N. Salama [*]

Sensors Lab, Advanced Membranes & Porous Materials Centre (AMPMC). Computer, Electrical and Mathematical Sciences and Engineering (CEMSE) Division, King Abdullah University of Science and Technology (KAUST), Thuwal, 23955-6900, Saudi Arabia

ARTICLE INFO

Keywords:
Laser-scribed graphene
Aptamer
Flexible electrodes
Biosensor
Breast cancer
Point-of-care testing

ABSTRACT

Improvements in the laser-scribed graphene (LSG)-based electrodes are critical to overcoming limitations of bare LSG electrodes in terms of sensitivity, direct immobilization of detection probes for biosensor fabrication, and ease of integration with point-of-care (POC) devices. Herein, we introduce a new class of nanostructured gold modified LSG (LSG-AuNS) electrochemical sensing system comprising LSG-AuNS working electrode, LSG reference, and LSG counter electrode. LSG-AuNS electrodes are realized by electrodeposition of gold chloride ($HAuCl_4$) solution, which gave~2-fold enhancement in sensitivity and electrocatalytic activity compared to bare LSG electrode and commercially available screen-printed gold electrode (SPAuE). We demonstrate LSG-AuNS electrochemical aptasensor for detecting human epidermal growth factor receptor 2 (Her-2) with a limit of detection (LOD) of 0.008 ng/mL and a linear range of 0.1–200 ng/mL. LSG-AuNS-aptasensor can easily detect different concentrations of Her-2 spiked in undiluted human serum. Finally, to show the LSG-AuNS sensor system's potential to develop POC biosensor devices, we integrated LSG-AuNS electrodes with a handheld electrochemical system operated using a custom-developed mobile application.

1. Introduction

The modern diagnostics technology revolution called "precision health" has already witnessed a widespread deployment and growing interest in point-of-care (POC) and wearable non- and minimally-invasive diagnostic devices (Ahmad et al., 2018; Gambhir et al., 2018; Heikenfeld et al., 2019; Ming et al., 2020; Ouyang et al., 2021; Sow et al., 2020; Williams et al., 2020; Yang et al., 2020). Early, low-cost, easy-to-use, and accurate POC detection of disease biomarkers is critical for managing global health issues. The world POC diagnostics market "is estimated to reach USD 46.7 billion by 2024 from USD 28.4 billion in 2019" (Markets And Markets, 2019). The main reason for the increase in POC devices' demand is the preference for rapid diagnosis at outpatient healthcare, hospitals, critical care centers, and home healthcare (Markets And Markets, 2019). Therefore, there is a high demand to develop new and improved diagnostic tools to meet end--users' growing needs and the POC market. Electrochemical biosensors have great potential to meet this demand due to their high specificity, accuracy, ease of use, and integration into handheld devices or mobile phone technology and the internet of things (IoT). For the development of electrochemical biosensors to meet the POC market's increasing demand, new electrodes that can be used to fabricate various sensing systems with improved electrochemical performance are highly desirable (da Silva et al., 2017).

Laser scribing of different substrates, such as polymers or graphene oxide, emerged as a new method for mask-free and straightforward 3D patterned graphene production (Dallinger et al., 2020; Lahcen et al., 2020). The production of laser-scribed graphene (LSG) or laser-induced graphene (LIG) electrodes using laser scribing of polyimide (PI) has been proved as a highly effective method of LSG production because of the low level of defects and large surface area due to the formation of stacked graphene flakes (Kurra et al., 2019; Lin et al., 2014; Nayak et al., 2016). LSG fabrication method creates flexible electrodes with fast and scalable fabrication without any mask or lithography equipment (Beduk et al., 2020; Lin et al., 2018a; Soares et al., 2020). A recent report showed that LSG electrodes provide many advantages such as mask-free

* Corresponding author.
E-mail address: khaled.salama@kaust.edu.sa (K.N. Salama).
[1] These authors contributed equally.

https://doi.org/10.1016/j.bios.2021.113116
Received 17 November 2020; Received in revised form 4 February 2021; Accepted 22 February 2021
Available online 27 February 2021

synthesis, 3D porous morphology, large surface area, fast electron mobility, cost-effectiveness, and high electrocatalytic activity as compared to commercially available screen-printed carbon electrodes, glassy carbon electrodes, and carbon paste electrodes (Ghanam et al., 2020).

Various enzymatic or non-enzymatic LSG-based sensors have been reported for the detection of different disease biomarkers, neurotransmitters, ions, bacteria, and other biomolecules (Lei et al., 2020; Lin et al., 2018b; Prabhakaran and Nayak 2020; Soares et al., 2020; Xu et al., 2018a; Yoon et al., 2020). Fenzl et al., (2017) reported a label-free voltammetric biosensor to detect coagulation factor thrombin using LSG as a working electrode, an Ag/AgCl reference electrode, and platinum wire as a counter electrode. Although these studies demonstrated LSG electrodes' potential for biosensor applications, for LSG electrodes to be qualified as POC electrochemical biosensor devices, a three-electrode system on the same chip is needed, and efforts in this direction will pave the way for the development of LSG-based POC devices. In this context, LIG or LSG electrodes were modified with gold, polyaniline (PA), reduced graphene oxide (rGO), and PA or rGO further modified with gold (Yu et al., 2018). In all cases, gold electroplating or polyaniline coating was carried out on interdigitated LSG electrodes using external platinum electrodes. Electrochemical impedance was used in combination with principal component analysis (PCA) to develop a multiflavor detection sensor (Yu et al., 2018). In another study, You et al., (2020), developed laser-induced noble metal nanoparticles (Au, Ag, and Pt) modified LIG electrodes using metal precursor-chitosan hydrogel ink coated on a polyimide substrate. These studies show a versatile method of producing different types of noble metal nanoparticle modified LIG electrodes and used electrochemical impedance spectroscopy (EIS) to detect pathogens.

According to the World Health Organization, female breast cancer is the second most frequently diagnosed cancer, with an 11.6% death rate, impacting 2.1 million women each year globally (WHO, 2020). The clinical diagnostics of breast cancer have gained tremendous attention recently, focusing on tissue-based biomarkers, including estrogen receptor (ER), progesterone receptor (PgR), Cytokeratin (CK), and human epidermal growth factor receptor 2 (Her-2) status (Sauter 2017). Among these biomarkers, Her-2 is the most crucial predictive marker in breast cancer (Colomer et al., 2018). Numerous biosensors have been reported to detect Her-2, employing different strategies and electrode types (Arya et al., 2018; Carvajal et al., 2018; Freitas et al., 2019; Ravalli et al., 2015). The development of POC diagnostics methods for the Her-2 biomarker and other cancer biomarkers is essential for detecting cancer at an early stage, which could significantly impact the cancer survival rate (Hayes et al., 2018).

Herein, for the first time, we report a gold nanostructured modified LSG based electrochemical aptasensor for the detection of Her-2 biomarker (Fig. 1). We used a simple electrodeposition technique to generate 3D gold nanostructures on the porous LSG electrode surface and obtained an excellent surface coverage of gold. Interestingly, our method produces a unique morphology of spiky and Christmas tree-like 3D shaped gold nanostructures present on the surface of LSG with better surface coverage, which are readily available for immobilization of biorecognition molecules. Due to gold's 3D nanostructures, the electron transfer rate was higher in LSG-AuNS electrodes than the simple LSG electrodes. These unique features enabled us to develop a low-cost, highly sensitive aptasensor with good reproducibility. The electrochemical biosensing system developed in these studies does not require printing an external Ag/AgCl reference electrode and platinum counter electrode for electrodeposition and biosensor applications. We also

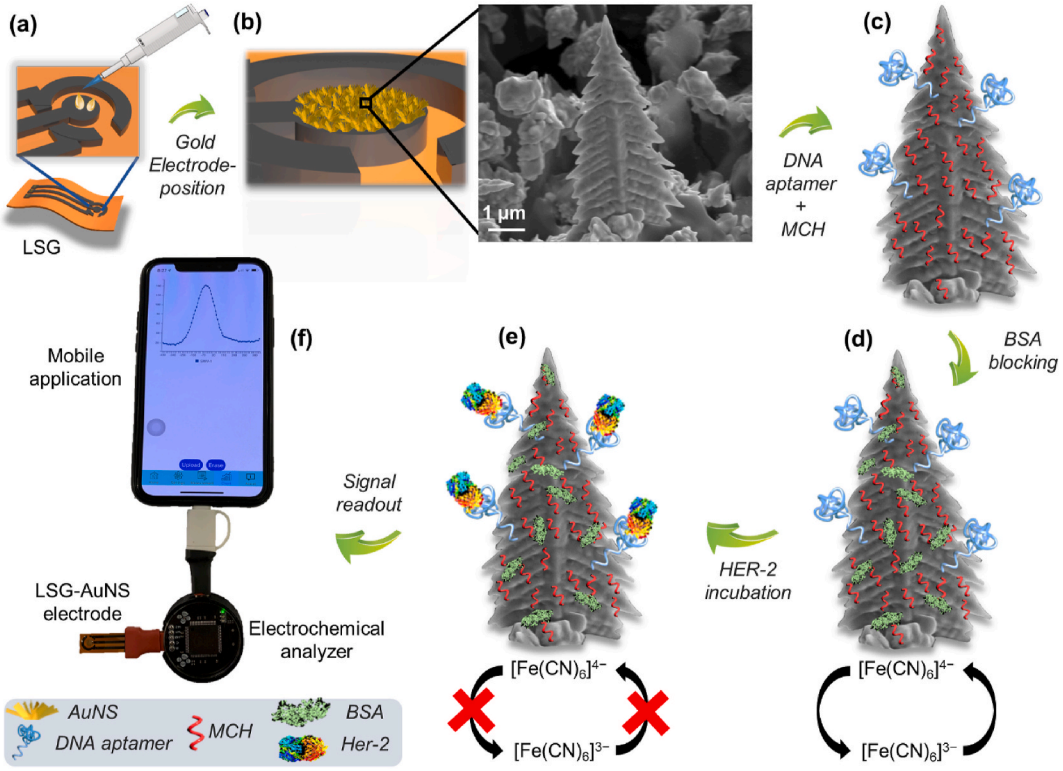

Fig. 1. Schematic illustration of the AuNS modified LSG-based aptasensor. (a, b) LSG electrode was first modified with AuNS. Spiky and Christmas tree-like gold nanostructures were formed (c) A mixture of Mercaptohexanol (MCH) and Thiol-modified DNA aptamer was immobilized onto the electrode surface. (d) Backfilling was carried out using a BSA solution to reduce non-specific adsorption. (e) The Her-2 solution was incubated onto the aptamer sensor. (f) The electrochemical signal was measured using a standard electrochemical work station, and custom made POC device before and after the binding of Her-2 from (d) and (e). The diffusion of the redox probe was hindered due to the binding of the Her-2 on the electrode surface resulting in the decrease in the peak current values, which correlated with the amount of Her-2 bound on the electrode surface. (For interpretation of the references to colour in this figure legend, the reader is referred to the Web version of this article.)

compared the electrochemically active surface area of the novel LSG-AuNS electrodes with the commercially available screen-printed gold electrodes (SPAuE). The obtained results indicated that LSG-AuNS electrodes have a high electroactive surface area thanks to the gold nanostructures and thus have promising potential as a platform for biosensing applications. As a demonstration of the application of the novel LSG-AuNS electrode system, we developed a highly sensitive and selective biosensor for Her-2 detection. LSG-AuNS-based aptasensor showed high affinity and specificity in the spiked human serum samples, which can be an excellent alternative to the existing complex sensors involving antibodies. Finally, we show the integration of LSG-AuNS electrodes in POC settings and demonstrate that this new system could be a potentially useful electrode system for developing POC diagnostics in the future.

2. Materials and methods

2.1. Chemicals and instrumentation

Thiol modified Anti-Her-2 DNA aptamer (APT): [ThiC6]AACCGCCCAAATCCCTAAGAGTCTGCACTTGTCATTTTGTATATGTATTTGGTTTTTGGCTCTCACAGACACACTACACACGCACA (Arya et al., 2018) was purchased from Sigma Aldrich. Gold (III) chloride hydrate ($HAuCl_4.xH_2O$), Hydrochloric acid (HCl), Mercaptohexanol (MCH), Cholesterol, Dopamine, Glucose, and Human Serum (H4522) were purchased from Sigma Aldrich. Cardiac Troponin-I (cTn-I) was purchased from Abcam. Potassium chloride (KCl), potassium ferricyanide (K_3 $[Fe(CN)_6]$), and potassium ferrocyanide (K_4 $[Fe(CN)_6]$) were purchased from MP Biomedicals. Her-2 protein was purchased from R & D systems UK. All chemicals were of analytical grade and used as received. The phosphate-buffered saline (PBS) tablets containing 0.0027 M potassium chloride (KCl) and 0.137 M sodium chloride (NaCl) with pH 7.4 were purchased from Fisher BioReagents. The ultrapure water (resistivity, 18.2 MΩ cm) from a Milli-Q® water purification system (Merck KGaA, Darmstadt, Germany) was used in all experiments. The screen printed-Au electrodes (SPAuE) were purchased from Methrom, Switzerland. Laser patterning was performed by using a CO_2 Universal Laser Systems®PLS6.75 laser with a laser spot diameter and wavelength of ~150 μm and 10.6 μm, respectively. The commercial PI substrate (Kapton Width:12") was purchased from Utech Products, USA, and used as the substrate. A Teneo VS scanning electron microscope (SEM) was used for the morphological characterization of the surface of different electrodes. All electrochemical experiments were performed by multiEmStat3-PalmSens electrochemical work station connected to a computer and controlled by MultiTrace software. Electrochemical Impedance Spectroscopy (EIS) measuremnts were carried-out using PalmSens 4 controlled with a PsTrace 5.8 software. A custom-made electrochemical POC device was used for square wave voltammetry (SWV) measurements for POC application.

2.2. LSG fabrication

LSG sensors were designed and fabricated as three-electrode systems with dimensions as length: 2.8 cm, width: 1.2 cm, and radius: 1.5 mm by CO_2 laser writing on a pre-cleaned PI sheet. All three LSG electrodes (working, reference, and counter) were fabricated on the same PI substrate. The scribing process was performed under inert gas flow to minimize the heteroatom binding to the graphene surface. The optimal laser scribing parameters used were 3.2 W power, 2.8 cm/s speed, 1000 pulses per inch, and 2.5 mm Z distance to obtain a relatively low sheet resistance value (58 Ω/square) (Beduk et al., 2020).

2.3. Electrochemical deposition of gold

The bare LSG electrodes were modified by electrochemical deposition using chronoamperometry, applying a constant potential of −0.9 V for 240 s in a solution containing 50 mM $HAuCl_4$ prepared in 0.5 M HCl as the electrolyte. Finally, 3D AuNS modified LSGs were rinsed with ultrapure water and dry with nitrogen gas (Fig. 1).

2.4. Aptamer immobilization onto LSG-AuNS and Her-2 detection

Stock solutions of DNA aptamer (100 μM) were prepared in TE buffer (10 mM TRIS, pH 8) and stored at −20 °C. The fresh working solutions of DNA aptamer were prepared using 10 mM PBS at pH 7.4 and were used immediately. The concentrated MCH solution was first prepared in ultrapure water and then further diluted in 10 mM PBS (pH 7.4). 4 μM of DNA aptamer was mixed with 20 μM of MCH prepared with 10 mM PBS (pH 7.4) to obtain a homogenized solution. As the next step, 6 μL from this mixture was placed onto each LSG-AuNS modified working electrode and incubated for 16 h. LSG-AuNS electrode surface was cleaned with 10 mM PBS (pH 7.4) to remove the excess of aptamer molecules and MCH. The aptasensor was incubated in 0.1 mg/mL of BSA solution in 10 mM PBS (pH 7.4) for 45 min to reduce non-specific adsorption. Finally, aptamer modified electrodes were washed with 10 mM PBS (pH 7.4) for at least five times. After the aptamer immobilization, 0.1, 1, 10, 50, 100, and 200 ng/mL of Her-2 were prepared in 10 mM PBS (pH 7.4) as the analyte and placed on top of the LSG-AuNS/aptamer electrodes for 1 h incubation. The electrodes were rinsed with PBS to remove non-bonded Her-2 and ready for the measurement step, as shown in Fig. 1. For the detection of Her-2 in undiluted serum, different concentrations of Her-2 were spiked into the serum and incubated onto the electrode surface for 1 h, and washed with 10 mM PBS (pH 7.4) before electrochemical measurements.

2.5. Electrochemical measurements

Cyclic voltammetry (CV) method with a scan rate of 100 mv/s and sweeping the potential from −0.6 V to +0.4 V and square wave voltammetry (SWV) method with a frequency of 2 Hz and sweeping the potential from −0.5 V to +0.5 V were used to study electrochemical responses of the LSG-AuNS/aptamer electrodes before and after interaction with Her-2. EIS parameters used were frequency 1.0 Hz to 100 kHz at 0 V. All electrochemical measurements were performed at room temperature in 0.1 M KCl containing 2.5 mM $[Fe(CN)_6]^{3-}/[Fe(CN)_6]^{4-}$ as a redox probe with LSG reference and counter electrodes. The changes in the current intensities are correlated to the different amounts of Her-2 captured by the DNA aptamer immobilized on the electrode surface. All electrochemical measurements were performed in triplicate.

3. Results and discussion

3.1. Electrochemical deposition of gold nanostructures on laser-scribed graphene

Fig. 2 (a-c) shows the optical, SEM images and Energy Dispersive X-ray Spectroscopy (EDX) characterization of the LSG, LSG-AuNS, and AuSPE electrodes. It can be seen (Fig. 2a) that the highly porous 3D structure of LSG was formed by the irradiation of the PI substrates, which is in agreement with the previous studies (Beduk et al., 2020; Fenzl et al., 2017; Soares et al., 2020). After the electrochemical deposition of gold on the LSG working electrode surface, we observed full surface coverage of the LSG working electrode by the gold nanostructures (AuNS) (Fig. 2b). Spiky and Christmas tree-like shapes were observed for AuNS deposited onto LSG compared to the commercially available SPAuE (Fig. 2c). The EDX results showed a clear peak attributed to elemental Au, confirming LSG electrode coverage by AuNS, and also, it is in agreement with the EDX spectra of commercially available AuSPE (Fig. 2a–c). We also tested electrodeposition of Palladium using Palladium chloride ($PdCl_2$) solution; however, this results in higher capacitive current (data not shown) compared to the AuNS electrode, and therefore, we did not explore this further. AuNS have been reported

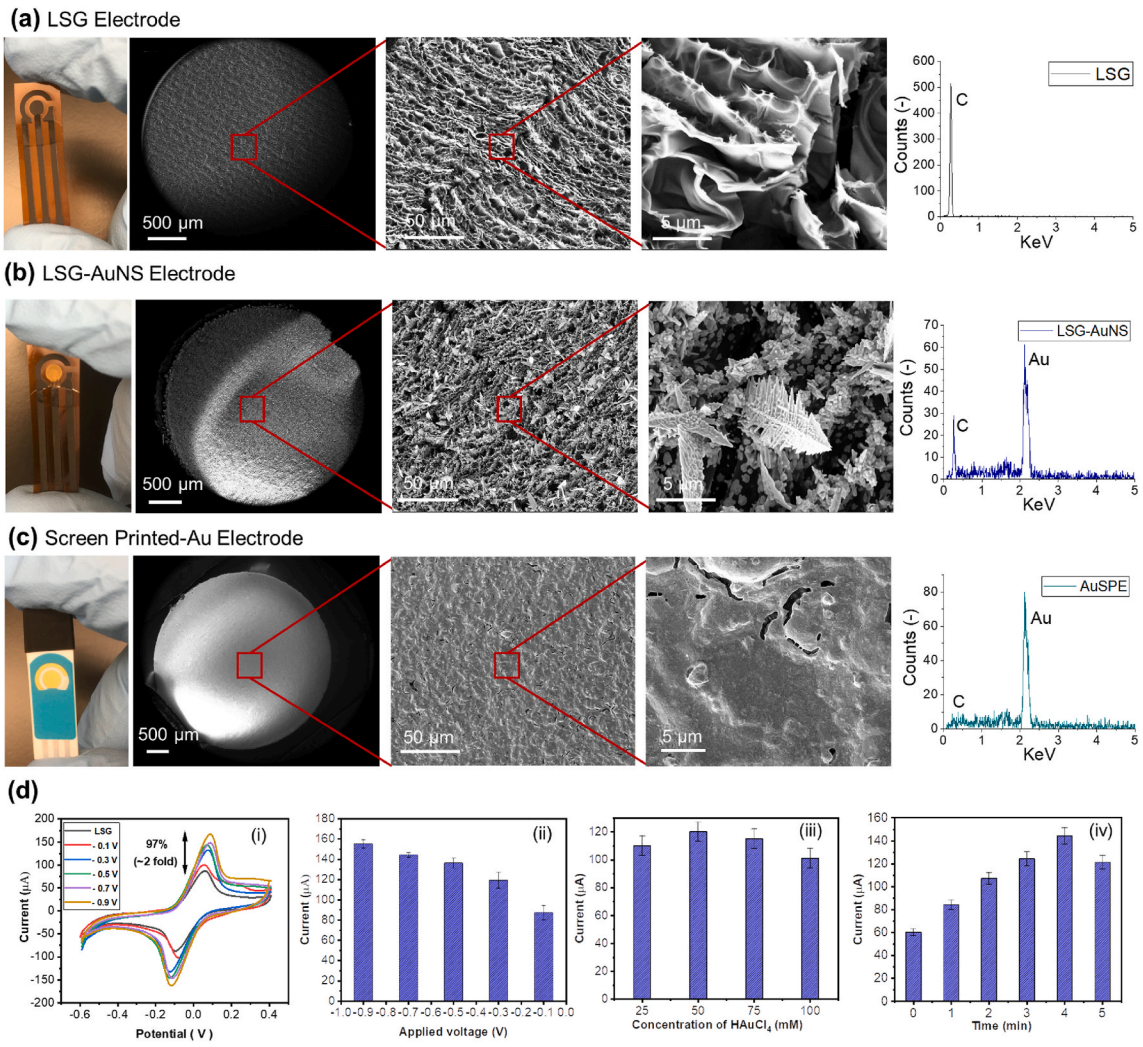

Fig. 2. Photographs, Scanning electron microscopy (SEM) images and EDX spectra of (a) LSG electrode (b) LSG-AuNS electrode and (c) Screen printed-Au electrode (SPAuE). Scale bar for SEM images from left to right: 500 μm, 50 μm, and 5 μm.(d), (i) Cyclic voltammograms obtained for LSG and LSG-AuNS electrodes prepared using electrochemical deposition of $HAuCl_4$ solution at different applied voltages in 0.1 M KCl containing 2.5 mM $[Fe(CN)_6]^{3-/4-}$, (ii) Histograms obtained for the effect of applied voltage on electrochemical response of LSG-AuNS electrode, (iii) Electrochemical response obtained for the LSG-AuNS electrodes prepared using different concentrations of $HAuCl_4$, and (iv) Effect of electrodeposition time on the electrochemical response of LSG-AuNS electrode. Error bars represent ±SD and n = 3 samples.

previously onto different types of macro and microelectrodes and showed great potential for the fabrication of various types of biosensors due to the large surface area and ease of modification of the electrode surface with detection probes (Besant et al., 2015; Mahshid et al., 2016; Shu et al., 2014; Soleymani et al., 2011). Considering the broader applications of gold nanostructured electrodes, we carried out the electrochemical deposition of gold onto LSG electrodes, including the reference and counter LSG electrodes, on the same chip. Several parameters were considered for the electrochemical deposition of AuNS, including the deposition time, the applied voltage, and the $HAuCl_4$ precursor concentration. We found that the applied voltage for electrochemical deposition profoundly affects the surface coverage of the LSG-AuNS electrode and its conductivity. We tested different potentials in the range of −0.1 V to −0.9 V for 180 s in a 50 mM solution of $HAuCl_4$. The cyclic voltammograms, presented in Fig. 2d (i), demonstrated the highest current response for the LSG-AuNS electrode prepared using −0.9 V. Approximately two-fold (97%) increase in the current response was observed after gold nanostructures deposition compared to the bare LSG electrode. As indicated in Fig. 2d (ii), the histogram shows that the increase in the applied potential (−0.1 V to −0.9 V) for the electrochemical deposition of gold increases the electrochemical response of the LSG-AuNS sensor. The SEM characterization also showed an incomplete deposition of gold from −0.1 V to −0.7 V, and full surface coverage was obtained at −0.9 V (Fig. S1).

We also studied the effect of $HAuCl_4$ concentration on the electrochemical performance of the LSG-AuNS electrodes. Different $HAuCl_4$ concentrations were used, such as 25 mM, 50 mM, 75 mM, and 100 mM. As can be seen in Fig. 2d (iii) and Fig. S2a, the results obtained showed the highest electrochemical response for the LSG-AuNS electrode prepared using 50 mM of $HAuCl_4$. This is due to the full coverage of the LSG working electrode surface by the AuNS, leading to a high electrocatalytic effect and large active surface area. However, after increasing the $HAuCl_4$ concentration beyond 50 mM, the electron transfer was hindered due to the agglomeration and formation of densely distributed AuNS (Shu et al., 2014). Notably, at higher concentrations, it was observed that some of the gold material was peeling off from LSG-AuNS electrodes. Hence, 50 mM of $HAuCl_4$ was chosen as the optimal value for the rest of the experiments. Another crucial parameter is the deposition time that affects the amount of the AuNS deposited and surface coverage. To optimize the deposition time, we fixed the concentration of gold and the applied voltage as 50 mM $HAuCl_4$ and -0.9 V, respectively. The AuNS electrodeposition time was varied from 1 to 5 min to study its

effect on the LSG-AuNS electrode performance. Fig. 2d (iv) and Fig. S2b show the obtained results for different electrodes prepared using different electrodeposition times. It can be seen that 4 min deposition time yields the highest electrochemical response compared to other LSG-AuNS electrodes prepared using different gold deposition times. Therefore, 4 min was chosen as the optimal value for the electrodeposition time for the rest of the experiments.

3.2. Effect of scan rate and flexibility test

The effect of the scan rate on the LSG and LSG-AuNS electrode prepared under optimal conditions was studied, as indicated in Fig. S3. The active surface area of the LSG-AuNS sensor was found to be 0.152 cm^2 that is greater than the LSG bare electrode 0.086 cm^2 and the one commercially available SPAuE (0.078 cm^2). The significant amplification of the active surface area is due to the high surface area of the AuNS deposited on the LSG working electrode and their excellent electrocatalytic effect. Thus, the LSG-AuNS electrode platform could serve as a potential candidate for developing highly sensitive electrochemical sensors and biosensors.

The LSG and LSG-AuNS electrodes' flexibility was also investigated by bending both electrodes at different angles for 1 min (Fig. S4). It was observed that the bending of the LSG and LSG-AuNS electrodes at ~45° and ~90° did not affect their electrochemical responses. Both LSG and LSG-AuNS electrodes responses remained almost unchanged, proving the new electrode platform's flexibility.

3.3. Electrochemical characterization of the aptasensor

The developed aptasensor was characterized using CV and EIS techniques to confirm the successful aptamer immobilization at the surface of the LSG-Au electrode. As shown in Fig. 3a, the sensor showed an approximately two-fold increase in the anodic current intensity after modifying the LSG electrode with the AuNS. This significant current increase is attributed to the high surface area of the AuNS, their excellent catalytic activity, and their high conductivity. These features facilitate the electron transfer at the interface between the LSG-AuNS electrode and electrolyte. After immobilization of the aptamer at the LSG-AuNS electrode, a significant decrease in the current intensity was observed, which confirmed the aptamer's successful immobilization on the electrode surface. The binding of Her-2 protein by the aptamer was confirmed by binding 100 ng/mL of Her-2. The difference in the current intensity after binding Her-2 was 51 ± 4.9 μA.

EIS measurements were also carried out to characterize the sensor surface modification steps, and the obtained results are summarized in Fig. 3b. Indeed, the EIS results were defined with the Nyquist diagram formed from Warburg impedance (W), resistances (Rs and Rct), and capacitance (C1). The EIS data are in agreement with the CV results (Fig. 3a). As the gold nanostructures (AuNS) were electrodeposited on top of the LSG working electrode surface, the Rct was dramatically decreased due to the high conductivity of AuNS. However, once the aptamer immobilized on the LSG-AuNS, the Rct increased, confirming aptamer's successful immobilization (Control). After Her-2 binding, a higher electron transfer resistance was observed due to the capture of Her-2 by the aptasensor, indicating its high affinity towards Her-2.

3.4. Optimization of the aptasensor

We tested the aptamer immobilization in the presence and absence of Mercaptohexanol (MCH). As shown in Fig. S5a, in the presence of MCH, the electrochemical response of the aptasensor was higher compared to the aptasensor response in the absence of MCH. The immobilization of DNA aptamer in the presence of MCH resulted in the proper folding and minimum steric hindrance of the DNA (Babelova et al., 2018; Keighley et al., 2008), which supports better attachment of Her-2 on the LSG-AuNS-DNA aptamer electrode surface. The incubation time is one of the essential parameters to optimize for the best performance of the aptasensor. In particular, we incubated the aptasensor in 10 mM PBS containing 100 ng/mL of Her-2 by varying the incubation time from 15 to 60 min, as presented in Fig. S5b. The aptasensor showed a measurable response after 15 min incubation time, and there was no statistically significant variation observed from 15 min to 60 min incubation time.

3.5. Sensitivity of the electrochemical aptasensor

Under the optimized experimental conditions, including the AuNS deposition, the immobilization of the aptamer, and the incubation time for Her-2 binding, we investigated the sensitivity of the developed aptasensor towards detecting the Her-2 protein. The proposed aptasensor showed a decrease in the electrochemical response of $[Fe(CN)_6]^{3-/4-}$ redox probe with the increase of Her-2 concentration (Fig. 4a). The decrease in the response of aptasensor with the increasing concentration of Her-2 is due to the hindrance in the diffusion of the redox probe to the electrode surface, i.e., the higher the amount of Her-2 bind to the electrode surface increases the hindrance in the diffusion process. Fig. 4b presents the corresponding calibration plot obtained for the LSG-AuNS aptasensor incubated in solutions of various Her-2 protein concentrations from 0.1 ng/mL to 200 ng/mL. Both sigmoidal curve fitting and logarithmic methods can be used to fit this type of data (Kutluk et al., 2020; Ou et al., 2020; Wang et al., 2018). As shown in Fig. 4b inset, a linear, logarithmic relationship was obtained, and the electrochemical response was increased with the increase in the concentration of Her-2 following the regression equation: $\Delta I_{ox} = 26.6 \log C_{Her\text{-}2} + 71.9$ with a correlation coefficient of 0.996. The limit of detection (LOD) was calculated to be 0.008 ng/mL using the above equation by defining log $C_{Her\text{-}2}$ equivalent to the average ΔI_{ox} of the blank plus three times its standard deviation (Ou et al., 2020; Patris et al., 2014; Wang et al., 2018; Xu et al., 2018b). The aptasensor

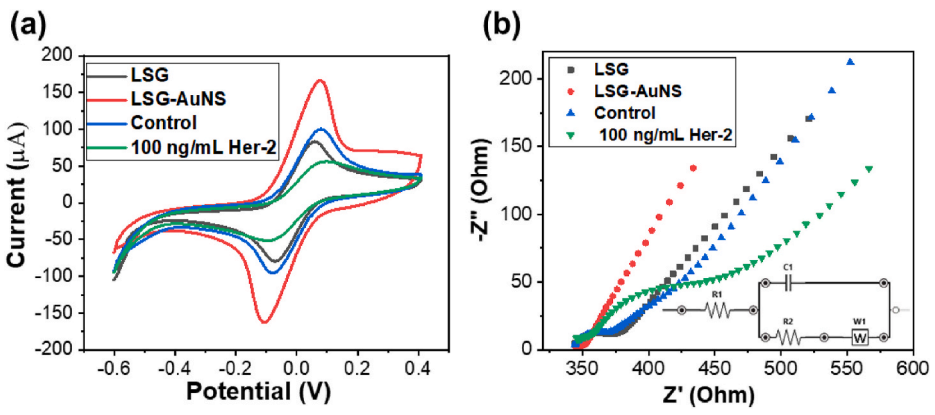

Fig. 3. (a) Cyclic voltammograms of bare LSG electrode, LSG-AuNS electrode, LSG-AuNS aptasensor (Control), and LSG-AuNS aptasensor after binding 100 ng/mL of Her-2. (b) Nyquist plots for bare LSG; LSG-AuNS, Control and after binding 100 ng/mL of Her-2. For EIS experiments only, external Ag/AgCl and Platinum counter electrodes were used. EIS parameters used were frequency 1.0 Hz to 100 kHz at 0 V. All the measurements were performed in 0.1 M KCl containing 2.5 mM $[Fe(CN)_6]^{3-/4-}$.

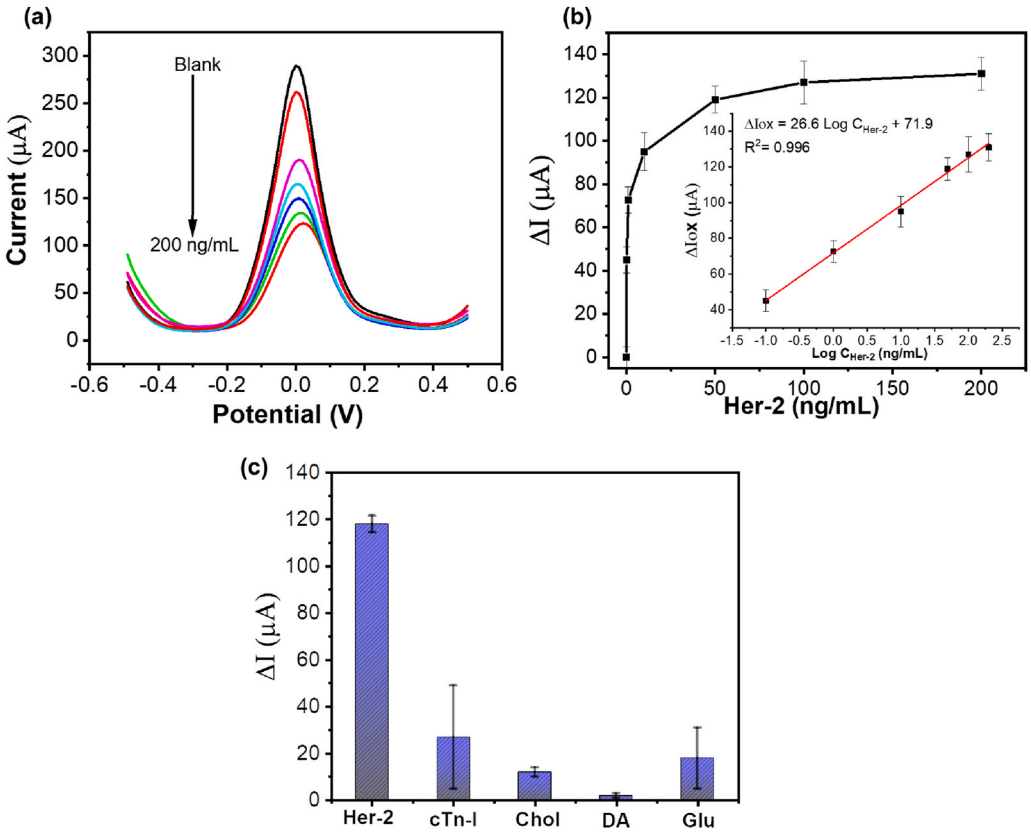

Fig. 4. (a) Square-wave voltammograms of LSG-AuNS aptasensor for different concentrations of Her-2 in 0.1 M KCl containing 2.5 mM $[Fe(CN)_6]^{3-/4-}$. Range of concentration used were Blank (0 ng/mL), 0.1, 1, 10, 50, 100 and 200 ng/mL, (b) Corresponding curve obtained from different Her-2 concentrations (0.1 ng/mL – 200 ng/mL). The inset graph shows the relationship between the ΔIox and the logarithm of Concentration of Her-2 (log C_{Her-2}). Error bars represent ±SD and n = 3 samples. (c) The response of the LSG-AuNS aptasensor in the presence of Her-2, cardiac Troponin-I (cTn-I), Cholesterol (Chol), Dopamine (DA), and Glucose (Glu). 50 ng/mL concentration was used for Her-2 and interfering molecules. Error bars represent ±SD and n = 3 samples.

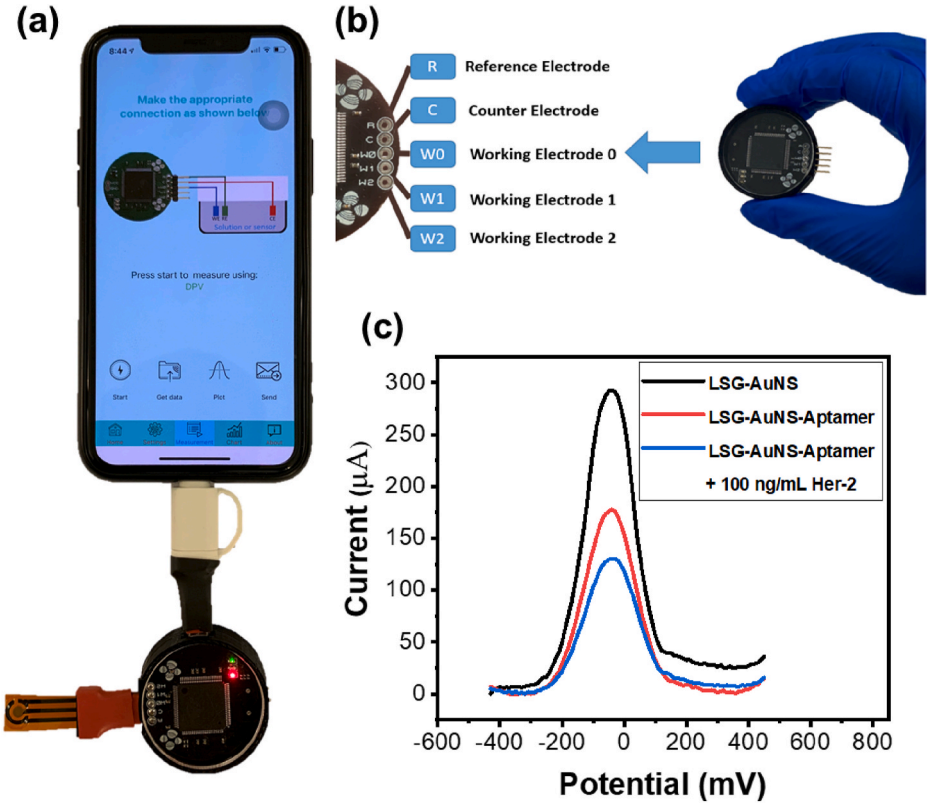

Fig. 5. (a, b) Shows the LSG-AuNS electrode's photograph integrated with a POC device operated using a custom-designed mobile application. KAUSTat is a polypotentiostat. The device has five pinouts: 3 working electrodes (WE), one reference electrode (RE), and one counter electrode (CE). The working electrodes can be switched to perform additional features, such as measuring voltage and current or even apply electrical signals. (c) Square-wave voltammograms of LSG-Au aptasensor measured using the POC device to detect 100 ng/mL of Her-2 in 0.1 M KCl containing 2.5 mM $[Fe(CN)_6]^{3-/4-}$.

developed in these studies showed comparable and in some cases superior analytical performance to detect Her-2 compared to many different strategies such as using screen-printed carbon electrodes, interdigitated gold microelectrodes, inkjet printed gold electrodes, and AuNPs modified graphite screen-printed electrodes reported previously (Table S1).

3.6. Selectivity studies

The interference of other possible biomolecules was studied by exploring the selectivity of the developed LSG-AuNS aptasensor. The affinity of the aptasensor was evaluated in the presence of some possible interferences, including Glucose (Glu), Cardiac troponin I (cTn-I), Cholesterol (Chol), and Dopamine (DA). The amounts of all interferences and Her-2 were fixed at 50 ng/mL. As shown in Fig. 5c, the proposed aptasensor exhibited high selectivity for the binding of Her-2 thanks to its high affinity to the aptamer. Significantly, low responses were obtained for Glu, Chol, and DA except for cTn-I, which is ~20% of the response of Her-2 with a large SD value. Among the interference molecules studied, cTn-I is a protein just like Her-2 with a different amino acid sequence and therefore has a higher tendency for non-specific attachment on the aptasensor surface. We have used a well-known MCH surface chemistry and BSA blocking strategy to reduce the non-specific adsorption (Babelova et al., 2018; Ferreira et al., 2021; Liu et al., 2012). However, Jolly et al., (2015) reported that changing the surface chemistry to sulfobetaine terminated thiol instead of MCH resulted in better antifouling properties of the aptasensor. Nonetheless, LSG-AuNS-aptasensor showed good selectivity towards detecting Her-2; this type of strategy would help further reduce the non-specific adsorption of the proteins on the LSG-AuNS aptasensor in the future.

To demonstrate the potential of LSG-AuNS aptasensor for the real sample application, we tested different amounts of Her-2 spiked in undiluted human serum. The clinically relevant cut-off value for Her-2 is 15 ng/mL (Carney et al., 2007). The value above 15 ng/mL considers as Her-2 positive and indicates tumor progression. Hence, serum samples were spiked with 0, 1, 10, 25, and 50 ng/mL of Her-2 to determine the recovery values using the SWV technique. As indicated in Table S2, for undiluted serum (0 ng/mL spiked Her-2), the recovered value was 0.07 ± 0.01 ng/mL, which may be attributed to the presence of intrinsic Her-2 and non-specific adsorption from serum proteins present in the serum sample used in these studies. A similar effect on the aptasensor signal was also observed by Arya et al., (2018) for detecting Her-2 in the undiluted human serum sample. The percentage recovery values for 1, 10, 25 and 50 ng/mL were 105, 116.9, 107 and 107.8%, respectively. The higher recovery values may be attributed to intrinsic Her-2 molecules in the undiluted serum and partly due to the non-specific adsorption of other molecules present in the serum sample. It is important to note that overall, the %RSD values become higher in undiluted serum samples spiked with Her-2 compared to %RSD values for PBS. Indeed, the obtained results demonstrated that LSG-AuNS aptasensor could discriminate easily between Her-2 positive and Her-2 negative in spiked human serum samples. These results show the potential of the developed aptasensor for the detection of Her-2 in patient samples.

3.7. Integration of LSG-AuNS electrode into point-of-care device

To show the potential of LSG-AuNS electrodes for the integration into POC devices, as a proof-of-concept, we conducted experiments using a second-generation custom-made POC electrochemical analyzer (KAUSTat) that operates directly from the phone battery with an in-house designed mobile application software which is compact and superior to the first generation KAUSTat (Ahmad et al., 2019). Fig. 5a and b, Fig. S6 and Fig. S7 show the details of the electrochemical measurement set-up of KAUSTat and the POC device's operation using the mobile application software. As shown in Fig. 5c, the SWVs indicate that LSG-AuNS electrodes integrated with the POC device can detect the presence of Her-2 in the sample compared to the control. We found that this POC device was less sensitive than the commercially available PalmSens electrochemical workstation used in these studies. However, as a proof-of-concept, it is evident that the LSG-AuNS electrodes can be integrated into POC devices to detect various disease biomarkers.

4. Conclusions

In summary, we reported a highly sensitive electrochemical biosensing system based on 3D-porous LSG electrodes modified with gold nanostructures. Our results showed a robust method to produce LSG based electrochemical system with better surface coverage, higher sensitivity, and ease of surface modification. As an example, we successfully demonstrated Her-2 cancer biomarker detection using the LSG-AuNS detection platform. The developed aptasensor allowed sensitive and selective detection of Her-2 in spiked human serum samples with satisfactory recoveries. Finally, as a proof of concept, we demonstrated LSG-AuNS sensing system integrated with a POC device that can be implemented to detect various disease biomarkers. The aptasensor showed some non-specific adsorption of proteins and an increase in the %RSD values in serum samples that can be improved by employing a better antifouling surface to block non-specific adsorption. The POC device's sensitivity needs improvement so that LSG-AuNS electrodes can be used to develop point-of-care testing devices in the future.

Author contributions

The manuscript was written through contributions of all authors. All authors have given approval to the final version of the manuscript.

CRediT authorship contribution statement

Sakandar Rauf: Methodology, Conceptualization, Validation, Formal analysis, Investigation, Writing – original draft, Visualization. **Abdellatif Ait Lahcen:** Methodology, Validation, Formal analysis, Investigation, Visualization, Writing – review & editing. **Abdulrahman Aljedaibi:** Investigation, Formal analysis, Writing – review & editing. **Tutku Beduk:** Investigation, Visualization, Writing – review & editing. **José Ilton de Oliveira Filho:** Investigation, Visualization, Writing – review & editing. **Khaled N. Salama:** Conceptualization, Methodology, Resources, Writing – review & editing, Supervision, Project administration, Funding acquisition.

Declaration of competing interest

The authors declare that they have no known competing financial interests or personal relationships that could have appeared to influence the work reported in this paper.

Acknowledgements

The authors would like to express their acknowledgements to the financial support of funding from King Abdullah University of Science and Technology (KAUST), Saudi Arabia. Also, we thank the KAUST Sensor Initiative and KAUST Visiting Student Research Program (VSPR) for supporting this work.

Appendix A. Supplementary data

Supplementary data to this article can be found online at https://doi.org/10.1016/j.bios.2021.113116.

References

Ahmad, R., Wolfbeis, O.S., Hahn, Y.B., Alshareef, H.N., Torsi, L., Salama, K.N., 2018. Deposition of nanomaterials: a crucial step in biosensor fabrication. Mater. Today Commun. 17, 289–321.

Ahmad, R., Surya, S.G., Sales, J.B., Mkaouar, H., Catunda, S.Y.C., Belfort, D.R., Lei, Y.J., Wang, Z.L., Baeumner, A., Wolfbeis, O.S., Alshareef, H.N., Salama, K.N., 2019. KAUSTat: a wireless, wearable, open-source potentiostat for electrochemical measurements. IEEE Sens. 19278454.

Arya, S.K., Zhurauski, P., Jolly, P., Batistuti, M.R., Mulato, M., Estrela, P., 2018. Capacitive aptasensor based on interdigitated electrode for breast cancer detection in undiluted human serum. Biosens. Bioelectron. 102, 106–112.

Babelova, L., Sohova, M.E., Poturnayova, A., Burikova, M., Bizik, J., Hianik, T., 2018. Label-free electrochemical aptasensor for jurkat cells detection as a potential diagnostic tool for leukemia. Electroanalysis 30 (7), 1487–1495.

Beduk, T., Lahcen, A.A., Tashkandi, N., Salama, K.N., 2020. One-step electrosynthesized molecularly imprinted polymer on laser scribed graphene bisphenol a sensor. Sensor. Actuator. B Chem. 314, 128026.

Besant, J.D., Das, J., Burgess, I.B., Liu, W.H., Sargent, E.H., Kelley, S.O., 2015. Ultrasensitive visual read-out of nucleic acids using electrocatalytic fluid displacement. Nat. Commun. 6, 6978.

Carney, W.P., Leitzel, K., Ali, S., Neumann, R., Lipton, A., 2007. HER-2/neu diagnostics in breast cancer. Breast Cancer Res. 9 (3), 207.

Carvajal, S., Fera, S.N., Jones, A.L., Baldo, T.A., Mosa, I.M., Rusling, J.F., Krause, C.E., 2018. Disposable inkjet-printed electrochemical platform for detection of clinically relevant HER-2 breast cancer biomarker. Biosens. Bioelectron. 104, 158–162.

Colomer, R., Aranda-Lopez, I., Albanell, J., Garcia-Caballero, T., Ciruelos, E., Lopez-Garcia, M.A., Cortes, J., Rojo, F., Martin, M., Palacios-Calvo, J., 2018. Biomarkers in breast cancer: a consensus statement by the Spanish society of medical oncology and the Spanish society of pathology. Clin. Transl. Oncol. 20 (7), 815–826.

da Silva, E.T.S.G., Souto, D.E.P., Barragan, J.T.C., Giarola, J.D., de Moraes, A.C.M., Kubota, L.T., 2017. Electrochemical biosensors in point-of-care devices: recent advances and future trends. Chemelectrochem 4 (4), 778–794.

Dallinger, A., Keller, K., Fitzek, H., Greco, F., 2020. Stretchable and skin-conformable conductors based on polyurethane/laser-induced graphene. ACS Appl. Mater. Inter. 12 (17), 19855–19865.

Fenzl, C., Nayak, P., Hirsch, T., Wolfbeis, O.S., Alshareef, H.N., Baeumner, A.J., 2017. Laser-scribed graphene electrodes for aptamer-based biosensing. ACS Sens. 2 (5), 616–620.

Ferreira, D.C., Batistuti, M.R., Bachour, B.J., Mulato, M., 2021. Aptasensor based on screen-printed electrode for breast cancer detection in undiluted human serum. Bioelectrochemistry 137, 107586.

Freitas, M., Nouws, H.P.A., Delerue-Matos, C., 2019. Electrochemical sensing platforms for HER2-ECD breast cancer biomarker detection. Electroanalysis 31 (1), 121–128.

Gambhir, S.S., Ge, T.J., Vermesh, O., Spitler, R., 2018. Toward achieving precision health. Sci. Transl. Med. 10 (430), eaao3612.

Ghanam, A., Lahcen, A.A., Beduk, T., Alshareef, H.N., Amine, A., Salama, K.N., 2020. Laser scribed graphene: a novel platform for highly sensitive detection of electroactive biomolecules. Biosens. Bioelectron. 168, 112509.

Hayes, B., Murphy, C., Crawley, A., O'Kennedy, R., 2018. Developments in point-of-care diagnostic technology for cancer detection. Diagnostics 8 (2), 39.

Heikenfeld, J., Jajack, A., Feldman, B., Granger, S.W., Gaitonde, S., Begtrup, G., Katchman, B.A., 2019. Accessing analytes in biofluids for peripheral biochemical monitoring. Nat. Biotechnol. 37 (4), 407–419.

Jolly, P., Formisano, N., Tkac, J., Kasak, P., Frost, C.G., Estrela, P., 2015. Label-free impedimetric aptasensor with antifouling surface chemistry: a prostate specific antigen case study. Sensor. Actuator. B Chem. 209, 306–312.

Keighley, S.D., Li, P., Estrela, P., Mighorato, P., 2008. Optimization of DNA immobilization on gold electrodes for label-free detection by electrochemical impedance spectroscopy. Biosens. Bioelectron. 23 (8), 1291–1297.

Kurra, N., Jiang, Q., Nayak, P., Alshareef, H.N., 2019. Laser-derived graphene: a three-dimensional printed graphene electrode and its emerging applications. Nano Today 24, 81–102.

Kutluk, H., Bruch, R., Urban, G.A., Dincer, C., 2020. Impact of assay format on miRNA sensing: electrochemical microfluidic biosensor for miRNA-197 detection. Biosens. Bioelectron. 148, 111824.

Lahcen, A.A., Rauf, S., Beduk, T., Durmus, C., Aljedaibi, A., Timur, S., Alshareef, H.N., Amine, A., Wolfbeis, O.S., Salama, K.N., 2020. Electrochemical sensors and biosensors using laser-derived graphene: a comprehensive review. Biosens. Bioelectron. 168, 112565.

Lei, Y.J., Alshareef, A.H., Zhao, W.L., Inal, S., 2020. Laser-scribed graphene electrodes derived from lignin for biochemical sensing. ACS Appl. Nano Mater. 3 (2), 1166–1174.

Lin, J., Peng, Z.W., Liu, Y.Y., Ruiz-Zepeda, F., Ye, R.Q., Samuel, E.L.G., Yacaman, M.J., Yakobson, B.I., Tour, J.M., 2014. Laser-induced porous graphene films from commercial polymers. Nat. Commun. 5, 5714.

Lin, S., Feng, W., Miao, X., Zhang, X., Chen, S., Chen, Y., Wang, W., Zhang, Y., 2018a. A flexible and highly sensitive nonenzymatic glucose sensor based on DVD-laser scribed graphene substrate. Biosens. Bioelectron. 110, 89–96.

Lin, X.N., Lu, Z.W., Dai, W.L., Liu, B.C., Zhang, Y.X., Li, J.Y., Ye, J.S., 2018b. Laser engraved nitrogen-doped graphene sensor for the simultaneous determination of Cd (II) and Pb(II). J. Electroanal. Chem. 828, 41–49.

Liu, B., Lu, L.S., Hua, E.H., Jiang, S.T., Xie, G.M., 2012. Detection of the human prostate-specific antigen using an aptasensor with gold nanoparticles encapsulated by graphitized mesoporous carbon. Microchim. Acta 178 (1–2), 163–170.

Mahshid, S., Mepham, A.H., Mahshid, S.S., Burgess, I.B., Safaei, T.S., Sargent, E.H., Kelley, S.O., 2016. Mechanistic Control of the growth of three-dimensional gold sensors. J. Phys. Chem. C 120 (37), 21123–21132.

Markets And Markets, 2019. Point of care diagnostics market. https://www.marketsandmarkets.com/. (Accessed 14 January 2021).

Ming, T., Luo, J., Liu, J., Sun, S., Xing, Y., Wang, H., Xiao, G., Deng, Y., Cheng, Y., Yang, Z., Jin, H., Cai, X., 2020. Paper-based microfluidic aptasensors. Biosens. Bioelectron. 170, 112649.

Nayak, P., Kurra, N., Xia, C., Alshareef, H.N., 2016. Highly efficient laser scribed graphene electrodes for on-chip electrochemical sensing applications. Adv. Electron Mater. 2 (10), 1600185.

Ou, X.Y., Pu, Q.L., Sheng, S.C., Dai, T., Gou, D., Yu, W., Yang, T.Y., Dai, L., Yang, Y.J., Xie, G.M., 2020. Electrochemical competitive immunodetection of messenger RNA modified with N6-methyladenosine by using DNA-modified mesoporous PtCo nanospheres. Microchim. Acta 187 (1), 31.

Ouyang, M., Tu, D., Tong, L., Sarwar, M., Bhimaraj, A., Li, C., Cote, G.L., Di Carlo, D., 2021. A review of biosensor technologies for blood biomarkers toward monitoring cardiovascular diseases at the point-of-care. Biosens. Bioelectron. 171, 112621.

Patris, S., De Pauw, P., Vandeput, M., Huet, J., Van Antwerpen, P., Muyldermans, S., Kauffmann, J.M., 2014. Nanoimmunoassay onto a screen printed electrode for HER2 breast cancer biomarker determination. Talanta 130, 164–170.

Prabhakaran, A., Nayak, P., 2020. Surface engineering of laser-scribed graphene sensor enables non-enzymatic glucose detection in human body fluids. ACS Appl. Nano Mater. 3 (1), 391–398.

Ravalli, A., da Rocha, C.G., Yamanaka, H., Marrazza, G., 2015. A label-free electrochemical affisensor for cancer marker detection: the case of HER2. Bioelectrochemistry 106, 268–275.

Sauter, E.R., 2017. Reliable biomarkers to identify new and recurrent cancer. Eur. J. Breast Health 13 (4), 162–167.

Shu, H.H., Cao, L.L., Chang, G., He, H.P., Zhang, Y.T., He, Y.B., 2014. Direct electrodeposition of gold nanostructures onto glassy carbon electrodes for non-enzymatic detection of glucose. Electrochim. Acta 132, 524–532.

Soares, R.R.A., Hjort, R.G., Pola, C.C., Parate, K., Reis, E.L., Soares, N.F.F., McLamore, E. S., Claussen, J.C., Gomes, C.L., 2020. Laser-induced graphene electrochemical immunosensors for rapid and label-free monitoring of Salmonella enterica in chicken broth. ACS Sens. 5 (7), 1900–1911.

Soleymani, L., Fang, Z.C., Lam, B., Bin, X.M., Vasilyeva, E., Ross, A.J., Sargent, E.H., Kelley, S.O., 2011. Hierarchical nanotextured microelectrodes overcome the molecular transport barrier to achieve rapid, direct bacterial detection. ACS Nano 5 (4), 3360–3366.

Sow, W.T., Ye, F., Zhang, C., Li, H., 2020. Smart materials for point-of-care testing: from sample extraction to analyte sensing and readout signal generator. Biosens. Bioelectron. 170, 112682.

Wang, Y., Cui, M., Jiao, M.X., Luo, X.L., 2018. Antifouling and ultrasensitive biosensing interface based on self-assembled peptide and aptamer on macroporous gold for electrochemical detection of immunoglobulin E in serum. Anal. Bioanal. Chem. 410 (23), 5871–5878.

WHO, 2020. WHO Report on Cancer: Setting Priorities, Investing Wisely and Providing Care for All. World Health Organization, ISBN 9789240001299.

Williams, N.X., Carroll, B., Noyce, S.G., Hobbie, H.A., Joh, D.Y., Rogers, J.G., Franklin, A. D., 2020. Fully printed prothrombin time sensor for point-of-care testing. Biosens. Bioelectron. 172, 112770.

Xu, G.Y., Jarjes, Z.A., Wang, H.W., Phillips, A.R.J., Kilmartin, P.A., Travas-Sejdic, J., 2018a. Detection of neurotransmitters by three-dimensional laser-scribed graphene grass electrodes. ACS Appl. Mater. Inter. 10 (49), 42136–42145.

Xu, Q.J., Wang, G.X., Zhang, M.M., Xu, G.Y., Lin, J.H., Luo, X.L., 2018b. Aptamer based label free thrombin assay based on the use of silver nanoparticles incorporated into self-polymerized dopamine. Microchim. Acta 185 (5), 253.

Yang, B., Fang, X.E., Kong, J.L., 2020. Engineered microneedles for interstitial fluid cell-free DNA capture and sensing using iontophoretic dual-extraction wearable patch. Adv. Funct. Mater. 30 (24), 2000591.

Yoon, H., Nah, J., Kim, H., Ko, S., Sharifuzzaman, M., Barman, S.C., Xuan, X., Kim, J., Park, J.Y., 2020. A chemically modified laser-induced porous graphene based flexible and ultrasensitive electrochemical biosensor for sweat glucose detection. Sensor. Actuator. B Chem. 311, 127866.

You, Z.H., Qiu, Q.M., Chen, H.Y., Feng, Y.Y., Wang, X., Wang, Y.X., Ying, Y.B., 2020. Laser-induced noble metal nanoparticle-graphene composites enabled flexible biosensor for pathogen detection. Biosens. Bioelectron. 150, 111896.

Yu, Y.C., Joshi, P.C., Wu, J., Hu, A.M., 2018. Laser-induced carbon-based smart flexible sensor array for multiflavors detection. ACS Appl. Mater. Inter. 10 (40), 34005–34012.